Effect of Magnesium Ions on the Tertiary Structure of the Hepatitis C Virus IRES and Its Affinity for the Cyclic Peptide Antibiotic Viomycin†

Siska Vos,‡ David J. Berrisford,§ and Johanna M. Avis*,‡

Department of Biomolecular Sciences and Department of Chemistry, UMIST, P.O. Box 88, Manchester M60 1QD, United Kingdom

Received August 1, 2001

ABSTRACT: A key ion-dependent folding unit within the hepatitis C IRES comprises the IIIef junction and pseudoknot. This region is also important in recruitment of the 40S ribosomal subunit. Here, circular dichroism is used to study the influence of metal ions on the structure and stability of this region. Comparison of the thermal stability of an IRES fragment encompassing subdomains IIIe/f and IV (named 3EF4) with that of a larger fragment also possessing subdomain IIId (3DEF4) indicates an additional stabilizing effect of Mg^{2+} ions on the latter fragment. Magnesium and potassium ions stabilize both fragments through nonspecific counterion effects. The additional effect of magnesium on 3DEF4, observed in the absence or presence of 100 mM KCl, is attributed to a nonspecific but high-affinity site for metal ions created by a region of unusual high charge density. Subdomain IIId presumably participates in tertiary packing interactions that provide such a site. Viomycin binds to the full-length IRES and RNA fragments with K_d values of 25−55 μM. Interestingly, viomycin binding to the two fragments is affected differently by Mg^{2+}; noncompetitive inhibition of binding to 3DEF4 is observed, whereas binding to 3EF4 is not impaired. Formation of a Mg^{2+}-stabilized tertiary fold, involving subdomain IIId, may thereby hinder viomycin binding to 3DEF4 indirectly. Mutational and deletion studies locate viomycin binding within subdomains IIIe/f rather than within the pseudoknot. In pseudoknot mutants, Mg^{2+} ions have different effects on viomycin binding and thermal stability, suggesting altered tertiary interactions involving subdomain IIId.

The hepatitis C virus (HCV)[1] is the main causative agent of non-A, non-B hepatitis in humans, posing a significant worldwide health threat. The virus has a positive-sense RNA genome of ∼9600 bases that exhibits considerable sequence diversity in the coding region (*1*). In contrast, the 5′ UTR and part of the 3′ UTR are strongly conserved in sequence, reflecting the requirement for conserved higher-order structures that play a role in translation and replication control (*2*, *3*). The 341-nucleotide (nt) 5′ UTR of the HCV genome contains a structured region that directly recruits the 40S small ribosomal subunit and is thus defined as an internal ribosome entry site (IRES), intimately involved in a non-cap-dependent mechanism of translation initiation (*4*−*6*).

The precise mechanism of translation initiation of the HCV genome is not resolved but appears to require only the IRES structure, eIF2, initiator tRNA, and eIF3 (*7*). The 5′ UTR of HCV has been divided into four structural domains, where domains II−IV form the IRES (Figure 1c) (*8*−*13*). Domains II and III are large complex secondary structures. A pseudoknot structure (*10*, *13*−*15*) is present at the base of domain III. Domain IV contains the initiator AUG codon and includes the first 11 nucleotides of the open reading frame (*9*). Domain III (specifically, an internal bulge in subdomain IIIb) is thought to interact with eIF3 during the initiation of translation and may help to recruit the ribosome to the IRES (*15*). However, it is possible for the ribosome to bind to the IRES in the absence of any other factor, suggesting the latter contains structural elements that allow direct recruitment and placement of the AUG start codon at the ribosomal P site (*16*, *17*). Primary ribosome−IRES interactions occur with subdomains IIId and IIIe/f and the pseudoknot structure (*15*, *16*). The helical junction IIIabc is also in the proximity of the 40S subunit (*17*), suggesting that this part of domain III might lie at the interface between the ribosomal subunit and eIF3 in the 43S preinitiation complex.

Overall, the IRES adopts an extended conformation within which helical junctions IIIabc and IIIef are key folding units (*18*−*20*). The fold at these junctions is dependent on divalent metal ions, and there is some evidence that loop IIId interacts with IIIe/f via long-range tertiary (3°) contacts (*18*). However, the RNA folds correctly in the presence of a variety of polyvalent cations, suggesting that a specific divalent metal ion is not required. High-resolution structural studies on the IRES are very limited. NMR structures of subdomains IIId and IIIe have been determined (*21*, *22*) in isolation from the folded IRES structure and, although informative, lack tertiary structure information. The remaining structural data are of

† This research was supported by a grant from the Biotechnology and Biological Sciences Research Council, United Kingdom (Grant 36/B10157).

* To whom correspondence should be addressed. E-mail: j.avis@umist.ac.uk. Telephone: +44-161-200-4216. Fax: +44-161-236-0409.

‡ Department of Biomolecular Sciences.

§ Department of Chemistry.

[1] Abbreviations: HCV, hepatitis C virus; IRES, internal ribosome entry site; UTR, untranslated region; CD, circular dichroism; PAGE, polyacrylamide gel electrophoresis.

10.1021/bi0156310 CCC: $22.00
Published on Web 04/03/2002

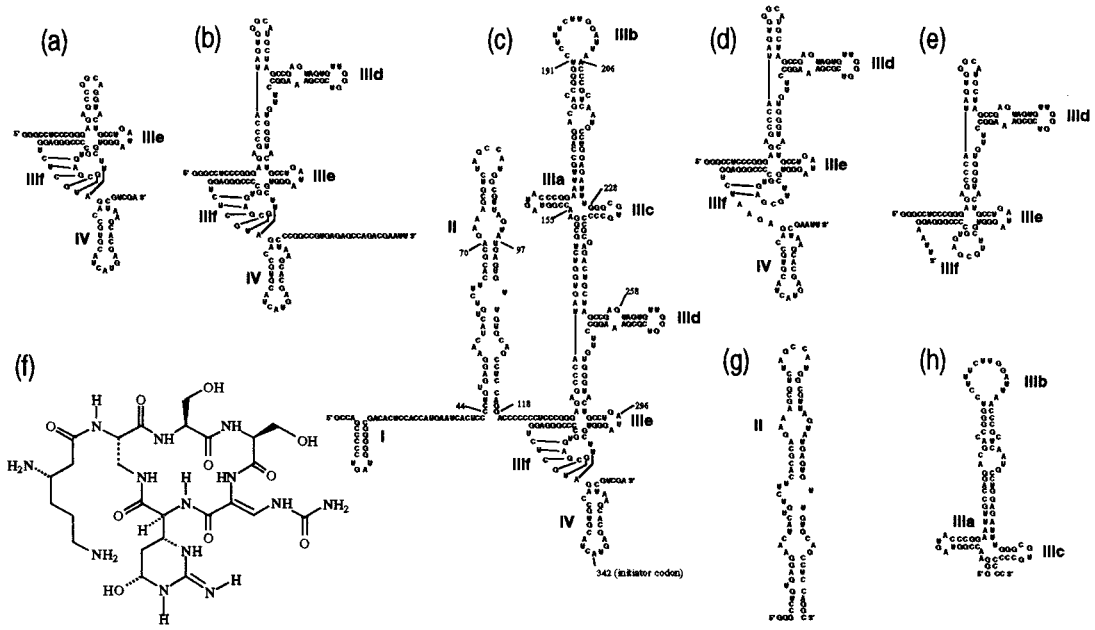

FIGURE 1: Secondary structure models of RNA molecules (based on that proposed in ref *9*) and viomycin used in this study: (a) fragment 3EF4, (b) fragment 3DEF4, (c) full-length IRES (termed WTIRES), (d) mutant 3DEΔ3F4, (e) mutant 3DEΔ3FΔ4, (f) viomycin, (g) fragment 2S, and (h) fragment 3ABC.

low resolution, arising primarily from cryoelectron microscopy of the full-length IRES bound to the rabbit 40S ribosomal subunit (*19*). Although of low resolution, these structural data are of some interest, confirming the IRES as an extended structure in which contacts to the ribosomal subunit are made primarily in the region of subdomains IIIe/f, the pseudoknot, and subdomain IV but also with subdomains IIIa and -c and the apical region of domain II.

Clearly, a better understanding of the tertiary structure in the region of the IIIef helical junction is crucial to gaining insight into a key component of the ribosome recognition and recruitment mechanism. Obtaining structural data on functionally important RNAs remains a significant challenge and is helped by a variety of experimental strategies. As one adjunct, small molecule ligands can serve as useful probes of RNA tertiary structure and protein−RNA interactions. In principle, such probes can then be developed through a process of structural analysis and synthetic modification into potential drug candidates. The area is now the subject of intense international interest, and the advances have been reviewed from a number of perspectives (*23*−*29*). It is within this context that many studies have focused on RNA recognition by the aminoglycosides, e.g., neomycin and analogues. Examples of biologically relevant RNAs that interact with aminoglycosides include ribosomal RNA (*30*), the TAT and RRE sequences of HIV-1 (*31*, *32*), and oncogenic RNA sequences (*33*). Recent structural work has greatly enhanced our understanding of the recognition process (*34*, *35*), at least with respect to neomycin and close analogues, but there remains a clear case for careful structural analysis of the recognition of medically relevant RNAs by both conventional and novel antibiotics. This information can be used to develop radically new antibiotics and to modify existing ones. Of particular relevance to HCV, inhibition of IRES RNA−protein interactions holds great potential for the development of new therapeutic strategies for this disease (*21*).

Another class of antibiotics known to bind specific RNAs consists of the tuberactinomycins. These are cyclic peptide compounds with relatively well defined conformations, of which the best characterized with respect to RNA recognition is viomycin (tuberactinomycin B, Figure 1f). Viomycin contains the unusual noncoded amino acids tuberactidine and ureidodehydroalanine in addition to β-lysine, serine, and diaminopropionic acid. It shows inhibitory effects on translation similar to those of aminoglycosides (*36*, *37*) and is a competitive inhibitor of the group I intron, HDV, and hammerhead ribozymes (*38*−*40*). Viomycin also induces interactions between RNA molecules. At subinhibitory concentrations, it switches the group I intron from a cis-acting to a trans-acting ribozyme (*41*). It can also enhance self-cleavage of the *Neurospora crassa* VS ribozyme and stimulate the trans cleavage reaction (*42*). Of particular interest to our study of the HCV IRES is the notable preference of viomycin for binding to pseudoknot structures in in vitro selection experiments (*43*, *44*).

In this study, we have investigated the structure and stability by circular dichroism of an independently folding unit within the HCV IRES. In particular, we have assessed the roles of subdomains IIId and IIIe/f, the pseudoknot, and subdomain IV in ion-dependent RNA folding by measuring the effect of magnesium and other metal ions on the thermal stability of RNA fragments encompassing this region. In addition, we have probed the RNA structures by measuring their affinity for viomycin, in the absence and presence of magnesium ions. We find that viomycin recognizes a specific RNA structure other than the pseudoknot. Furthermore, binding of viomycin to the RNA is very different from the binding of metal ions, the former being precluded when magnesium ions are present due to ion-dependent changes in the tertiary structure of the RNA involving subdomain IIId.

MATERIALS AND METHODS

Materials. All chemicals were analytical grade. All solutions were prepared using water treated with diethyl pyrocarbonate. Restriction enzymes and *Taq* DNA polymerase were obtained from Roche Ltd. Ribonucleotides were purchased from Sigma, and their solutions were adjusted to pH 8.0 with concentrated NaOH. T7 RNA polymerase was prepared in-house from the plasmid pT7-911 as described previously (*45*). Viomycin sulfate was purchased from Research Diagnotics, Inc.

Cloning of HCV Genome Fragments for RNA Production. DNA fragments encoding the RNA molecules shown in Figure 1 were prepared by PCR amplification of the appropriate regions of the HCV IRES in plasmid pCR3.1HCV5′UTR. The PCR primers incorporated an *Sph*I restriction site and a T7 promoter directly upstream of the fragment and an *Eco*RI restriction site directly downstream of the fragment, in the case of 3DEF4, 3DEΔ3F4, 3DEΔ3FΔ4, and WTIRES, and *Sal*I in the case of 3EF4. The PCR mixtures contained each primer at 0.5 mM, 25 ng of pCR3.1HCV5′UTR, 0.25 mM dNTPs, 1.5 mM $MgCl_2$, and 0.025 unit of *Taq* DNA polymerase. Fragments were cloned into the plasmid pHST07 between the *Sph*I and *Eco*RI or *Sal*I sites and sequenced using the Perkin-Elmer BigDye sequencing protocol.

RNA Synthesis and Purification. For in vitro transcription reactions, the pHST07 plasmid containing the cloned insert was linearized using *Eco*RI or *Sal*I and purified by extraction with phenol and chloroform (pH 8.0) and 2-propanol precipitation. Transcription reactions were typically carried out in 1−5 mL, and the mixtures contained 80 mM HEPES (pH 7.5), 2 mM spermine, 40 mM DTT, 25 mM $MgCl_2$, 7 mM rNTPs, 100 μg/mL linearized plasmid, 2.5 mg/mL T7 RNA polymerase, 2 units/mL yeast inorganic pyrophosphatase, and 4% (v/v) RNAsecure (Ambion Ltd.). Prior to addition of the enzymes, the reaction mixtures were heated to 60 °C for 10 min and then cooled to room temperature. Reaction mixtures were incubated at 37 °C for 3 h, and the RNA was purified immediately by phenol/chloroform (1:1) extractions at pH 6.6 and then at pH 4.7. The RNA was precipitated using 2-propanol at −20 °C. RNA precipitates were immediately redissolved since dried pellets were difficult to dissolve. To remove all traces of salts, metal ions, and unincorporated rNTPs, the RNA fragments were resuspended in formamide containing 10 mM EDTA and heated in a boiling water bath for several minutes. The samples were then extensively dialyzed in succession against 8 M urea containing 10 mM EDTA, 10 mM EDTA, and finally H_2O. Purified RNA preparations were stored at −20 °C.

RNA fragments were analyzed on 4% polyacrylamide/bisacrylamide (19:1) gels containing 8 M urea and 1× TBE. Samples were diluted 2-fold with loading buffer (deionized formamide containing 100 mM EDTA, 5 mg/mL xylene cyanol, and 5 mg/mL bromophenol blue) and boiled for several minutes before immediate loading onto a pre-electrophoresed gel. Electrophoresis (36 W) was continued until bromophenol blue had migrated through three-quarters of the gel. RNA was visualized by ethidium bromide staining.

Renaturation of RNA Fragments and Analysis on Native PAGE. Optimal renaturation procedures for the RNA fragments used in this study were identified from CD studies (described below). To the purified RNAs was added HEPES (pH 7.5) to a final concentration of 10 mM, and aliquots of up to 300 μL were transferred to PCR tubes. The RNA fragments were renatured in a PCR machine using the following protocol; tubes were heated to 90 °C at a rate of 0.01 °C/s, held at 90 °C for 1 min, and then cooled to 4 °C at 0.01 °C/s. Renatured RNA solutions were stored at 4 °C. Renatured RNA fragments were analyzed on 4% polyacrylamide/bisacrylamide (19:1) gels buffered with 75 mM Tris-glycine (pH 7.5). Gels also contained 2 mM $MgCl_2$ when the effect of Mg^{2+} on RNA structure was being analyzed. To test the effect of viomycin on the RNA structures, the samples were preincubated with 10 μM to 1 mM viomycin sulfate for 15 min at room temperature prior to gel analysis. Gels were pre-electrophoresed for a minimum of 15 min at 100 V, and sample electrophoresis was then carried out at 4 °C until the bromophenol blue had migrated through three-quarters of the gel. RNA was visualized by staining with ethidium bromide and UV transillumination.

Circular Dichroism Studies. Circular dichroism (CD) studies were carried out in a Jasco J-810 CD spectropolarimeter equipped with a Jasco Peltier-type temperature control system (model PTC-423S/L) connected to a Grant W6 circulating water bath. Samples typically contained 10 μM RNA, 10 mM HEPES (pH 7.5), and 0 or 100 mM KCl, as well as the required ligand, either 0−20 mM $MgCl_2$, 0−200 μM viomycin sulfate, or one of the metal ion solutions [$CaCl_2$, $CoCl_2$, $MnCl_2$, or $Co(NH_3)_6Cl_3$] at either 100 μM or 1 mM, in a final volume of 250 μL. Samples were prepared in a 1 mm CD quartz cuvette with a lid to prevent evaporation during heating.

Spectra were measured from 350 to 200 nm at 0 °C, using a 1 nm bandwidth, a 1 s response time, and a data pitch of 0.2 nm. Spectra were averaged over two to four accumulations. Melting curves were measured by monitoring the CD at 265 nm, using a 1 nm bandwidth, a 1 s response time, and a data pitch of 0.2 °C. Samples were heated from 0 to 90 °C at 1 °C/min, and renatured to 0 °C at the same rate. Heating of samples at a rate of 0.5 °C/min produced an identical denaturation curve, establishing that a thermal equilibrium was attained.

The denaturation profiles of both 3EF4 and 3DEF4 show a single, large transition taking place over the 90 °C temperature range (see the Results). This transition is likely to represent the sum of the many individual transitions that take place during unfolding. In this study, we have not attempted to quantitate the thermal parameters that describe each of the transitions. For qualitative analysis, the midpoint of the observed major transition, T_m, was calculated using the following expression

$$\mathrm{CD} = \frac{m_L T + b_L}{1 + K} + \frac{(m_H T + b_H)K}{1 + K} \qquad (1)$$

where m_L and b_L are the slope and intercept, respectively, of the low-temperature baseline and m_H and b_H are the those of the high-temperature baseline. K is the equilibrium constant for the folding to unfolding transition, defined by the equation $K = e^{\Delta H/R(1/T_m + 1/T)}$, where R is the gas constant (*52*).

For CD studies using viomycin, the denaturation profile was corrected for background CD due to viomycin, since the signal due to viomycin changes linearly upon heating.

Microcalorimetry. Binding constants for viomycin binding to the RNA fragments and full-length IRES in the presence of varying $MgCl_2$ concentrations at 25 °C were measured in an isothermal titration microcalorimeter (MicroCal Inc., model VP-ITC). Renatured RNA (1−5 μM) in 10 mM HEPES (pH 7.5) and $MgCl_2$ or KCl at the appropriate concentration were placed into the sample chamber. Viomycin sulfate at 0.25−1 mM in 10 mM HEPES (pH 7.5), containing the same concentration of $MgCl_2$ or KCl, filled the injection syringe. Viomycin was injected into the sample chamber in 1 × 2 μL aliquot, and then in 20 × 10 μL aliquots. The heat liberated as a result of each injection was measured for 400 s.

Microcalorimetry data were analyzed using the program WinCF (Kevin Raner Software, http://www.home.aone.net.au/krs). The data were converted by summating the heat of binding, Q_i, for each ith injection to give the total heat released, Q_{total}, for m injections

$$\langle Q_{total} \rangle = \sum_{i=1}^{m} \langle Q_i \rangle$$

The binding of viomycin to RNA can be written as follows

$$R + V \rightleftharpoons RV$$

where R is the RNA, V is viomycin, and RV is the RNA−viomycin complex. The equilibrium constant, K_a, is given by

$$K_a = \frac{[RV]}{[R][V]}$$

The fraction of RNA to which viomycin has bound is the ratio of the total amount of heat liberated after m injections, Q_{total}, to the maximum amount of heat that can be liberated in the experiment, Q_{max}, and can be expressed as

$$\frac{Q_{total}}{Q_{max}} = \frac{K_a[V]}{1 + K_a[V]}$$

Q_{max} is not measured in the experiment but is one of the parameters fitted to the data.

Several of the RNA fragments exhibited a slight sigmoidal response to viomycin binding, indicating some cooperativity. For these binding data, the binding equation was modified to include a Hill coefficient, n, as follows

$$\frac{Q_{total}}{Q_{max}} = \frac{K_a[V]^n}{1 + K_a[V]^n}$$

Several of the binding experiments also reveal a second viomycin binding event which is characterized by a linear increase in Q_{total}. This second binding event may be viomycin binding with a dissociation constant that is much higher than the range of viomycin concentrations used in the experiments. However, we have interpreted this secondary binding as nonspecific association of viomycin to the RNA and model it as a straight line. The expression used in the fitting of parameters to the microcalorimetry binding data is therefore

$$Q_{total} = \frac{Q_{max}K_a[V]}{1 + K_a[V]} + u[V] \quad (2)$$

where $u[V]$ corresponds to nonspecific binding. The parameter u was set to zero in those experiments where nonspecific binding was not detected. For analysis of the inhibition data (below), the nonspecific binding component, $u[V]$, was subtracted from the total heat of binding, Q_{total}, using the fitted value for u, to give the heat of binding for the first binding event.

For noncompetitive inhibition, Mg^{2+} ions bind to RNA and the RNA−viomycin complex as given by

$$R + Mg \rightleftharpoons R{\cdot}Mg$$

$$RV + Mg \rightleftharpoons RV{\cdot}Mg$$

where R·Mg is magnesium ion bound to RNA and RV·Mg is magnesium ion bound to the RNA−viomycin complex.

The inhibitor association constants are given by

$$K_i^{R\cdot Mg} = \frac{[R{\cdot}Mg]}{[R][Mg]} \text{ and } K_i^{RV\cdot Mg} = \frac{[RV{\cdot}Mg]}{[RV][Mg]}$$

The total amount of RNA, R_t, is

$$[R] + [RV] + [R{\cdot}Mg] + [RV{\cdot}Mg] = R_t$$

The fraction of RNA to which viomycin has bound, $\bar{\upsilon}$, can therefore be expressed as

$$\bar{\upsilon} = \frac{[RV]}{R_t} = \frac{[RV]}{[R] + [RV] + [R{\cdot}Mg] + [RV{\cdot}Mg]}$$

Substituting for [RV], [R·Mg], and [RV·Mg] and dividing by [R] gives

$$\bar{\upsilon} = \frac{K_a[V]}{1 + K_a[V] + K_i^{R\cdot Mg}[Mg] + K_i^{RV\cdot Mg}K_a[V][Mg]}$$

For graphical analysis, the above equation can be linearized by taking the reciprocal of both sides

$$\frac{1}{\bar{\upsilon}} = 1 + K_i^{RV\cdot Mg}[Mg] + \left(\frac{1}{K_a} + \frac{K_i^{R\cdot Mg}[Mg]}{K_a}\right)\frac{1}{[V]} \quad (3)$$

Plots of the slope and y-intercept of each line fitted in the double-reciprocal plot against $MgCl_2$ concentration will allow estimation of the inhibition binding constants for $MgCl_2$ using the expressions

$$K_i^{R\cdot Mg} = \frac{\text{slope}_{slope}}{y\text{-intercept}_{slope}} \text{ and } K_i^{RV\cdot Mg} = \text{slope}_{y-\text{intercept}} \quad (4)$$

RESULTS

Experimental Strategy and RNA Molecules Used in Our Study. The RNA molecules used in our study are based on the secondary structure model that has been proposed for the HCV IRES (*8*), and are named according to the domains that they include. The entire 5′ UTR of the hepatitis C RNA genome, which incorporates the IRES, is contained within the fragment termed WTIRES (nucleotides 1−354, Figure 1c). The smallest RNA fragment (termed 3EF4, nucleotides

125−139 and 285−354, Figure 1a) encompasses subdomains IIIe and IIIf and domain IV of the IRES, while the larger RNA fragment (termed 3DEF4, nucleotides 125−144 and 249−354, Figure 1b) also incorporates subdomain IIId and has an additional 24 nt tail of non-HCV sequence at its 3′ end. We have also studied two pseudoknot mutants (termed 3DEΔ3F4 and 3DEΔ3FΔ4, panels d and e of Figure 1, respectively). In the mutant 3DEΔ3F4, the center three of the six predicted Watson−Crick base pairings within the pseudoknot stem have been mutated to destabilize the formation of the pseudoknot. The mutations are in the same three positions as in a previous study where mutagenesis at these positions was shown, by enzymatic structure probing and functional assays, to disrupt stem formation (*10*). The second mutant, 3DEΔ3FΔ4, lacks the strand which forms the pseudoknot, as well as downstream sequences.

A primary objective is to study the structure and global thermal stability of these RNA molecules using circular dichroism, to observe the influence of various metal ions on this stability, and to assess the binding of viomycin to the different fragments. We have particularly focused on the region of the pseudoknot and the IIIef helical junction since this is an independently folding unit that is structurally poorly resolved, yet is an important component of the interaction with the 40S ribosomal subunit. The RNA fragments are necessarily rather large and will, therefore, present a thermal melting profile with numerous transitions that are difficult or impossible to resolve. Hence, our strategy is to compare the effect of metal ions on the global stability of fragments and thus assign some differences in the melting profiles to the presence or absence of helical segments. Analysis of viomycin binding to the fragments allows us to establish whether this region of the IRES possesses a high-affinity site for this molecule, a molecule that has precedence for binding pseudoknot structures (*43*, *44*). The effects of metal ions on viomycin binding and the combination of these data with the metal ion stability analyses should give insight into the RNA tertiary structure in this region and the mode of ligand binding.

Two other RNA fragments which incorporate other domains within the HCV IRES have also been characterized for viomycin binding. These are termed 2S, which corresponds to domain II, and 3ABC, which corresponds to subdomains IIIabc (panels g and h of Figure 1, respectively).

Production of RNA and Analysis on Denaturing and Native PAGE. Transcription reactions typically yielded ∼5 mg of pure RNA per 1 mL of reaction mixture. Correctly renatured RNA was assumed to be where the sample migrated as a single band on native PAGE, and aggregation of the RNA in the well was minimal (Figure 2). The WTIRES and 3EF4 RNA fragments migrated as a single band when the RNA fragments were renatured in 10 mM HEPES (pH 7.5) (Figure 2a, lanes 2 and 3), either in the absence or in the presence of 2 mM MgCl. Upon renaturation in the same buffer (no $MgCl_2$), fragments possessing subdomain IIId (3DEF4 and mutants) presented extra bands (Figure 2a, lanes 1, 4, and 5) of faster migration. The extra bands were more prominent in the case of the mutant pseudoknot fragments. In the presence of 2 mM $MgCl_2$, 3DEF4 and 3DEΔ3FΔ4 now migrate as a single band (Figure 2b, lanes 1 and 3), suggesting full conformational homogeneity. Mutant 3DEΔ3F4, however, migrates as at least three bands in the presence of

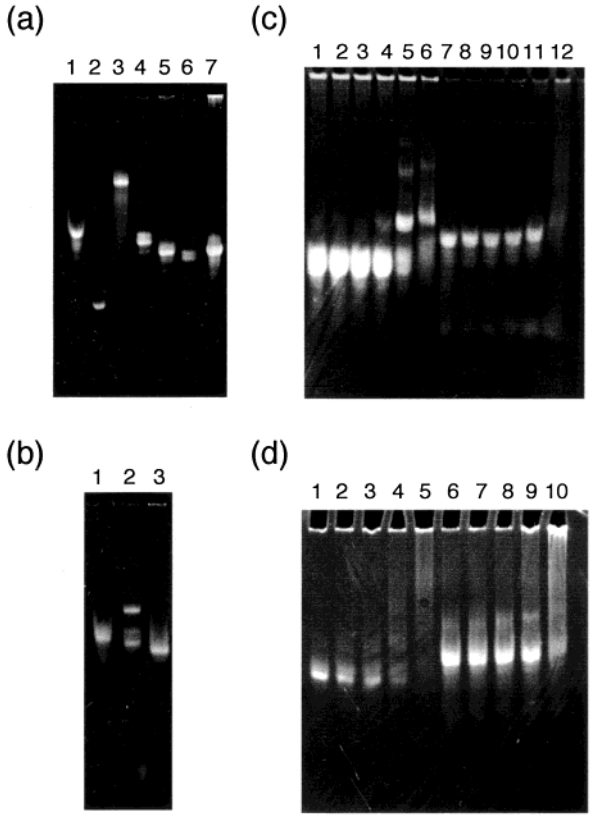

FIGURE 2: Native PAGE analysis of renatured RNA fragments. (a) RNA electrophoresed in the absence of $MgCl_2$: lane 1, 3DEF4; lane 2, 3EF4; lane 3, WTIRES; lane 4, 3DEΔ3F4; lane 5, 3DEΔ3FΔ4; lane 6, 2S; and lane 7, 3ABC. (b) RNA electrophoresed in the presence of 2 mM $MgCl_2$: lane 1, 3DEF4; lane 2, 3DEΔ3F4; and lane 3, 3DEΔ3FΔ4. (c) Testing of viomycin-induced RNA aggregation: lanes 1−6, 3DEF4 at 3.9 μM in 0, 10 μM, 50 μM, 100 μM, 250 μM, and 1 mM viomycin, respectively; and lanes 7−12, 3EF4 at 7.9 μM in 0, 10 μM, 50 μM, 100 μM, 250 μM, and 1 mM viomycin, respectively. (d) Testing of viomycin-induced RNA aggregation in the presence of 2 mM $MgCl_2$: lanes 1−5, 3DEF4 at 3.9 μM in 0, 50 μM, 100 μM, 250 μM, and 1 mM viomycin, respectively; and lanes 5−10, 3EF4 at 3.9 μM in 0, 50 μM, 100 μM, 250 μM, and 1 mM viomycin, respectively.

$MgCl_2$ (Figure 2b, lane 2), of which the upper one is probably a higher-molecular weight aggregate such as a dimer. For all RNA fragments, the same results were obtained whether $MgCl_2$ was included before or after the renaturation process. The native PAGE analysis is important as it establishes that the RNAs can be renatured into single species (assuming that aggregates are stable to the electrophoresis conditions). They also demonstrate that, with the exception of one mutant fragment (3DEΔ3F4), Mg^{2+} ions do not cause RNA aggregation, thus excluding this possibility when Mg^{2+} ions are present in thermal stability analyses.

Assessing RNA Structures by CD. Circular dichroism was used to study RNA structure and the changes that occur upon thermal melting and/or renaturation and addition of metal ions. The CD spectra of renatured 3EF4 and 3DEF4 exhibit two major peaks centered at 265 and 209 nm (Figure 3). These peaks are due to $\pi-\pi^*$ electronic transitions in the stacked planar bases, influenced by the asymmetric 3′-endo sugar rings (*46*). The wavelengths of the peaks are characteristic of RNA in an A-form helical conformation. In addition to these two peaks, the spectra also show a smaller peak centered at 223 nm. The CD spectra of 3EF4, 3DEF4

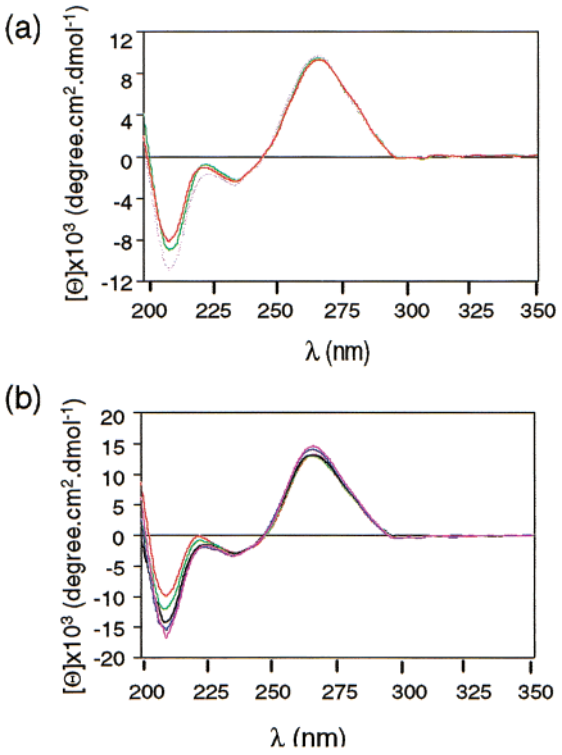

FIGURE 3: CD spectra of 3EF4 (a) and 3DEF4 (b) fragments measured in varying concentrations of $MgCl_2$. Samples contained ~10 μM RNA, 10 mM HEPES (pH 7.5) and either 0 (red), 1 (green), 2 (black), 3 (lavender) 5 (blue), or 20 mM $MgCl_2$ (pink).

(Figure 3), and WTIRES (not shown) change significantly when $MgCl_2$ is added to the RNA. The CD change is assumed to reflect the conformational change in the RNA induced by Mg^{2+} ion binding. The magnitudes of both the peaks at 265 and 209 nm increase when $MgCl_2$ is added, indicating increased helix structure and base stacking, while the magnitude of the peak at 223 nm decreases.

Denaturation of 3EF4 and 3DEF4 Is Reversible. By following the decrease in the CD signal at 265 nm upon heating from 0 to 90 °C, the melting profile for both 3EF4 and 3DEF4 in the absence of metal ions appears as a broad transition with a midpoint (apparent T_m) at ~45 °C (Figure 4a,c). Individual transitions during unfolding cannot be resolved; hence, CD studies are used only to give some insight into Mg^{2+}- or ligand-dependent changes to the RNA structure. Renaturation of the RNA was also monitored upon sample cooling. The denaturation and renaturation profiles are superimposable, demonstrating a reversible process (data not shown).

Mg^{2+} Ions Stabilize both 3DEF4 and 3EF4 RNA during Denaturation. The effect of $MgCl_2$ on the denaturation profile of 3DEF4 is shown in Figure 4a. There is a noticeable effect on the broad transition between 1 and 2 mM $MgCl_2$. The apparent T_m increases from 45 °C at low Mg^{2+} concentrations (<1 mM) to ~84 °C at high concentrations (>2 mM), with an apparent midpoint of stabilization at ~1.1 mM $MgCl_2$. The results suggest that there is stabilization of the RNA tertiary structure by Mg^{2+} ions, since lower-temperature unfolding transitions have shifted to a temperature range that overlaps with unfolding of the RNA secondary structure. Addition of $MgCl_2$ up to a concentration of 20 mM to the RNA did not further affect the denaturation profile; however, some hydrolysis is apparent in samples containing >10 mM $MgCl_2$.

Denaturation studies on a 10-fold concentration range of 3DEF4 (3−30 μM) in the presence of varying $MgCl_2$ concentrations have shown that the midpoint of stabilization by $MgCl_2$ is consistently in the range of 1.1−1.2 mM $MgCl_2$ (data not shown). Stabilization is not, therefore, due to

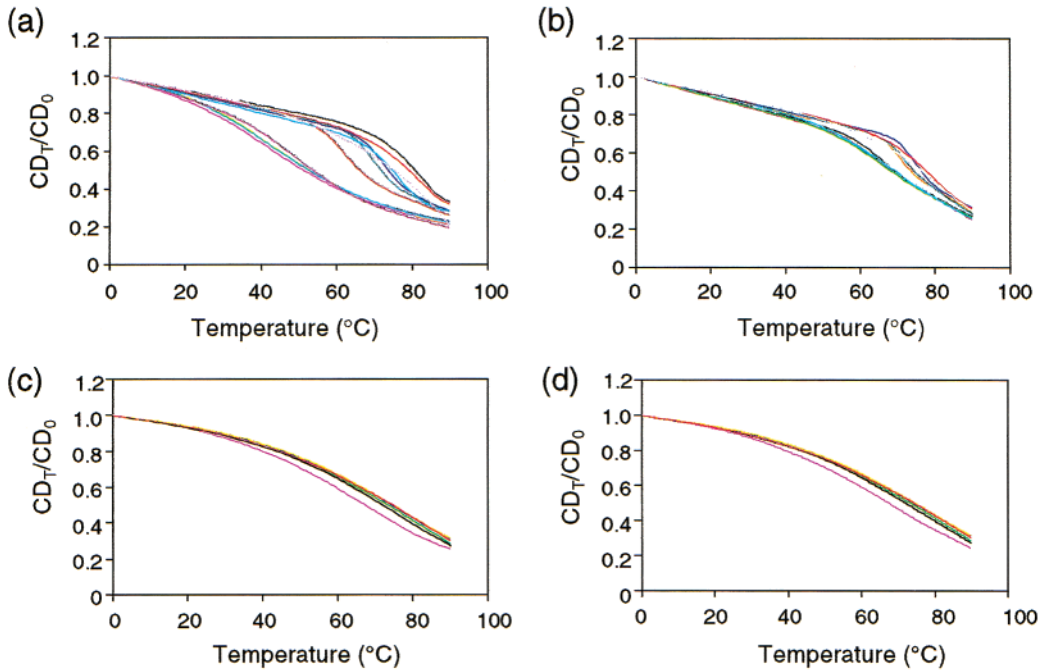

FIGURE 4: Effect of $MgCl_2$ and KCl on 3DEF4 and 3EF4 denaturation. (a) Denaturation of 3DEF4 in the presence of either 0 (dark blue), 0.05 (pink), 0.25 (yellow), 1 (light blue), 1.05 (violet), 1.1 (dark red), 1.2 (dark green), 1.3 (dark blue), 1.5 (sky blue), 2 (black), 5 (red), or 10 mM $MgCl_2$ (lavender). (b) Denaturation of 3DEF4 in 100 mM KCl in the presence of either 0 (dark blue), 1 (violet), 2 (black), 2.1 (green), 2.2 (light blue), 2.25 (orange), 2.3 (dark green), 3 (blue), 5 (red), or 10 mM $MgCl_2$ (lavender). (c) Denaturation of 3EF4 in the presence of either 0 (pink), 1 (black), 2 (green), 5 (red), or 10 mM $MgCl_2$ (yellow). (d) Denaturation of 3EF4 in 100 mM KCl in the presence of either 0 (pink), 1 (black), 2 (green), 5 (red), or 10 mM $MgCl_2$ (yellow).

magnesium-induced aggregation of the RNA. This conclusion is supported by native PAGE analysis of 3DEF4 in 2 mM $MgCl_2$ (Figure 2b) and the reversibility of denaturation observed for this fragment in the presence of varying $MgCl_2$ concentrations.

Although potassium ions (100 mM KCl) also stabilize 3DEF4 RNA during thermal denaturation (the apparent T_m increases to 80 °C; Figure 4b), and Mg^{2+} ions do not further increase this apparent T_m, an additional effect of Mg^{2+} ions on the RNA structure is evident through observation of the sharpening of the transition curve. In this case, this occurs when the $MgCl_2$ concentration is between 2 and 2.3 mM and again suggests RNA tertiary structure stabilization by Mg^{2+} ions. Mg^{2+} ions also stabilize 3EF4 against thermal denaturation (Figure 4c), although the effect is not as dramatic as that observed with 3DEF4 and no significant further effect of Mg^{2+} is observed in the presence of 100 mM KCl (Figure 4d). The Mg^{2+}-induced effects on the thermal stability of the larger 3DEF4 fragment are thus attributed to the presence of the extra subdomain in this fragment, namely, IIId. Mg^{2+} ions appear to affect a structural transition involving this subdomain.

Viomycin Stabilizes both 3DEF4 and 3EF4 to Denaturation. CD was used to investigate whether binding of the cyclic peptide antibiotic viomycin to the HCV IRES fragments alters the conformation and stability of these molecules. The addition of 0−200 μM viomycin sulfate to either 3DEF4 or 3EF4 RNA has no effect on their CD spectra under all the conditions that were investigated. However, viomycin produces an effect on the denaturation profiles of 3DEF4 RNA similar to that produced by addition of $MgCl_2$ (Figure 5), the apparent T_m for unfolding increasing to approximately 85 °C at 200 μM viomycin sulfate. The concentration of viomycin required to induce this effect is thus at least 50-fold lower than that of Mg^{2+} ions. However, due to the absorbance of viomycin itself at 265 nm, 200 μM was the maximum concentration that could be tested and maximum stabilization of 3DEF4 by viomycin may not yet have been attained. Since we are able to monitor only a broad transition, the structure made more resistant to thermal denaturation by viomycin need not necessarily be the same structure as that stabilized by Mg^{2+} ions. A stabilizing effect is not surprising given the positively charged functional groups on viomycin that confer counterion properties upon it. However, a contribution to RNA stabilization arising from structure-selective binding is a possibility as discussed later.

Viomycin also stabilizes the 3EF4 fragment, interestingly to a greater degree than Mg^{2+} ions. The melting transitions were not complete at 90 °C, thus preventing the fitting of T_m values to these denaturation curves. The presence of 100 mM KCl with either RNA during denaturation removes the stabilizing effects of viomycin (data not shown) for both RNA fragments. In this respect, indications are that magnesium ions and viomycin do not mediate their effects on RNA stability through identical means. The similar effects of viomycin on the stability of the two fragments also support this suggestion, when contrasted with the quite distinct effects of magnesium ions.

Viomycin Binding to 3EF4 and 3DEF4 Is Affected Differently by Magnesium Ions. To probe the nature of RNA recognition by viomycin, constants for binding to the different RNA fragments were measured by isothermal titration microcalorimetry (Figures 6 and 7) and the effects of metal ions on binding examined. The results are summarized in Table 1. A better fit to the data measured for 3DEF4 was achieved when a Hill coefficient (fitted as 1.1) was included in the minimization. In the absence of $MgCl_2$ (Figure 6), viomycin binds to both RNA fragments, the mutants, and WTIRES, with similar affinities (K_d = 25−55 μM). The data suggest that viomycin binds preferentially to a site in the IRES within subdomains IIIe/f and domain IV. Binding is significantly weaker (Figure 7d and Table 1) to fragments representing domain II and subdomains IIIabc (Figure 1g,h), providing further evidence that WTIRES and fragments 3DEF4 and 3EF4 incorporate a relatively high-affinity binding site for viomycin in their structure.

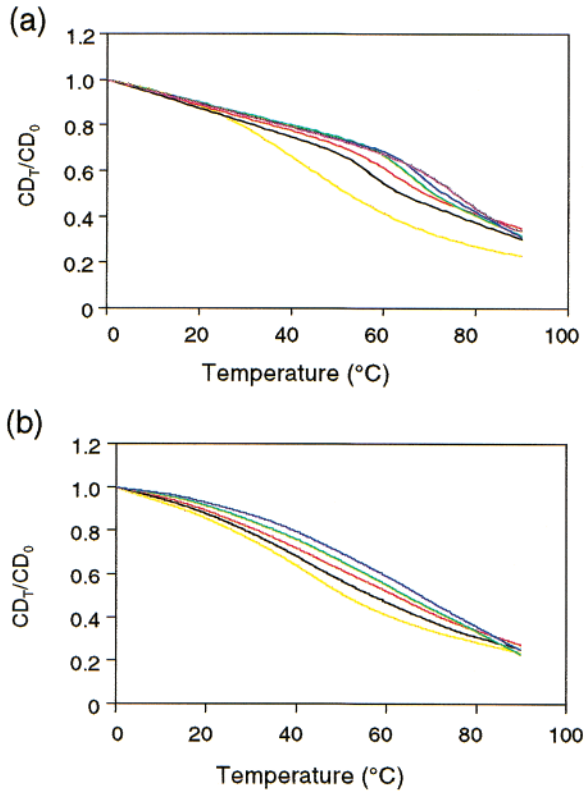

FIGURE 5: Effect of viomycin in 3DEF4 and 3EF4 denaturation. (a) Denaturation of 3DEF4 in the presence of either 0 (yellow), 20 (black), 40 (red), 60 (green), 100 (blue), or 200 μM viomycin sulfate (violet). (b) Denaturation of 3EF4 in the presence of either 0 (yellow), 20 (black), 40 (red), 60 (green), or 100 μM viomycin sulfate (blue). The denaturation curves have been adjusted for the change in CD due to viomycin itself.

The presence of $MgCl_2$ has different effects on the binding of viomycin to the two pseudoknot RNA fragments. In the case of 3DEF4, the heat of binding, Q_{max}, is reduced as the $MgCl_2$ concentration is increased, while the K_d for viomycin remains largely unchanged (Figure 6a and Table 1). This is indicative of $MgCl_2$ inhibiting viomycin binding in a noncompetitive manner. The apparent inhibition constants, $K_i^{R\cdot Mg}$ and $K_i^{RV\cdot Mg}$, are found to be in the same range at 3.7 and 4.3 mM^{-1}, respectively. This indicates that magnesium ions exert the same effect on both free and viomycin-complexed RNA. The apparent dissociation constant for $MgCl_2$ causing this inhibitory effect was calculated, from $1/K_i$, to be ~0.3 mM. In the case of addition of $MgCl_2$ to 3EF4 RNA during viomycin binding experiments, the K_d for viomycin remains largely unchanged and Q_{max} increases with

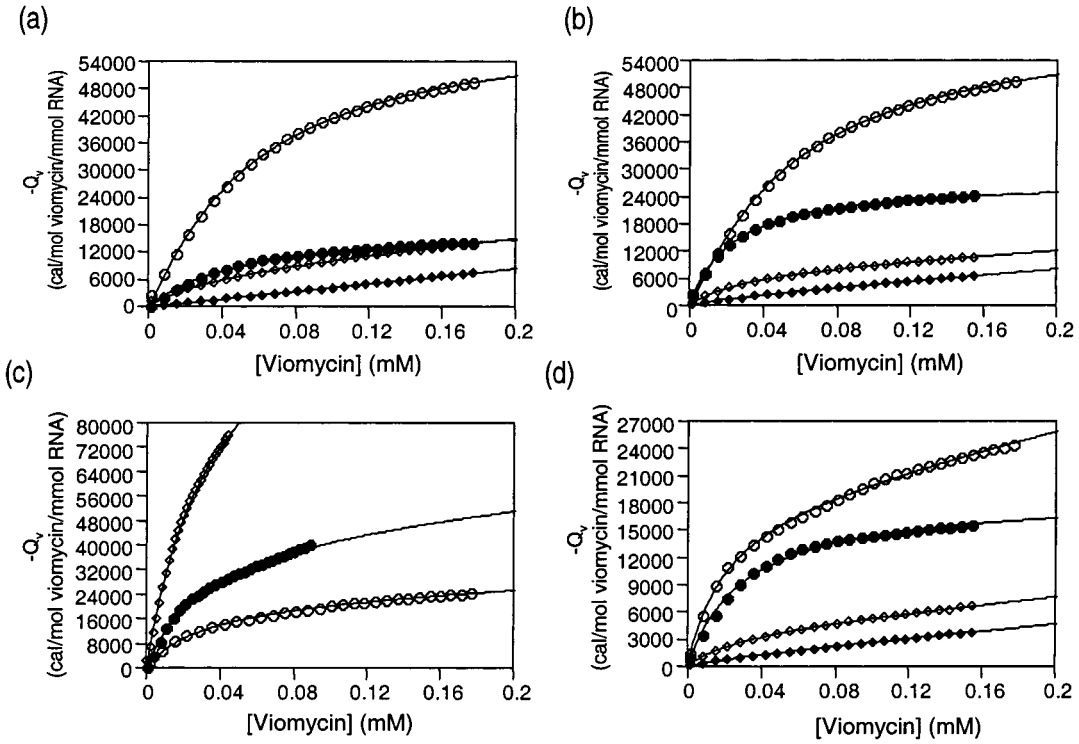

FIGURE 6: Viomycin binding to 3DEF4 and 3EF4 in the presence of varying $MgCl_2$ and KCl concentrations. (a) Viomycin binding to 3DEF4 in the absence of $MgCl_2$ (○) and in the presence of 0.5 mM $MgCl_2$ (●), 1 mM $MgCl_2$ (◇), and 5 mM $MgCl_2$ (◆). (b) Viomycin binding to 3DEF4 in the absence of KCl (○) and in the presence of 10 mM KCl (●), 50 mM KCl (◇), and 100 mM KCl (●). (c) Viomycin binding to 3EF4 in the absence of $MgCl_2$ (○) and in the presence of 1 mM $MgCl_2$ (●) and 5 mM $MgCl_2$ (◇). (d) Viomycin binding to 3EF4 in the absence of KCl (○) and in the presence of 10 mM KCl (●), 50 mM KCl (◇), and 100 mM KCl (◆). K_a values were fitted according to eq 2 and are given in Table 1.

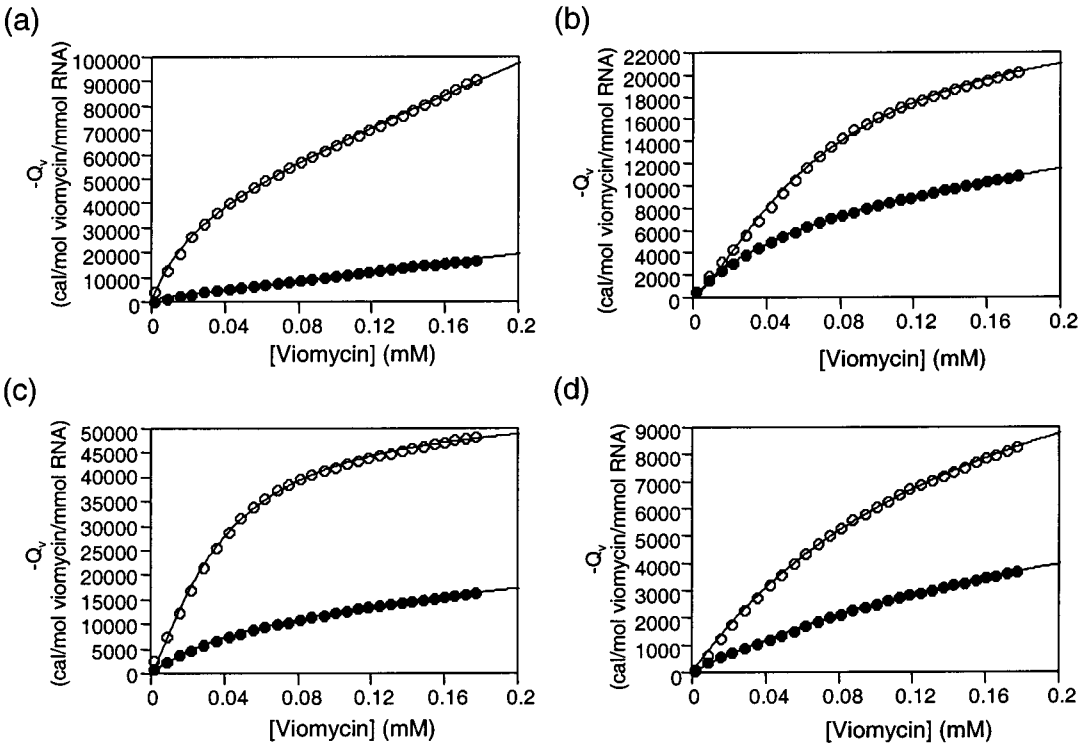

FIGURE 7: Viomycin binding to various RNA fragments. (a) Viomycin binding to WTIRES in the absence of $MgCl_2$ (○) and in the presence of 1 mM $MgCl_2$ (●). (b) Viomycin binding to 3DEΔ3F4 in the absence of $MgCl_2$ (○) and in the presence of 1 mM $MgCl_2$ (●). (c) Viomycin binding to 3DEΔ3FΔ4 in the absence of $MgCl_2$ (●) and in the presence of 1 mM $MgCl_2$ (●). (d) Viomycin binding to fragments 2 (●) and 3ABC (○) in the absence of $MgCl_2$. K_a values were fitted according to eq 2 and are given in Table 1.

increasing $MgCl_2$ concentrations (Figure 6c and Table 1). The apparent dissociation constant for $MgCl_2$ here is ~6 mM.

The effect of the presence of 1 mM $MgCl_2$ on the binding of viomycin to WTIRES was similar to that observed for

Table 1: Binding Constants for Viomycin

RNA	[KCl] (mM)	[Mg^{2+}] (mM)	K_a (mM^{-1})	$-Q_{max}$ (kcal/mol)	K_d (μM)	n^b
3DEF4	0	0	18.03 ± 0.56	169.67 ± 2.56	55.46 ± 1.72	1.1
	0	0.5	26.82 ± 1.27	46.06 ± 0.65	37.29 ± 1.77	–
	0	1	23.21 ± 4.14	24.62 ± 3.02	43.08 ± 7.69	–
	0	5	NS[a]	NS[a]	NS[a]	–
	10	0	37.98 ± 0.78	47.67 ± 0.47	26.33 ± 0.54	1.24
	50	0	33.04 ± 3.17	11.79 ± 0.70	30.27 ± 2.90	–
	100	0	20.88 ± 1.53	3.03 ± 0.17	47.89 ± 3.51	–
3EF4	0	0	32.97 ± 3.11	45.86 ± 2.48	30.33 ± 2.86	–
	0	1	31.52 ± 5.33	93.64 ± 13.18	31.73 ± 5.36	–
	0	5	26.71 ± 0.70	278.80 ± 4.09	37.44 ± 0.98	–
	10	0	41.74 ± 0.81	52.28 ± 0.46	23.96 ± 0.46	0.98
	50	0	31.25 ± 2.31	17.54 ± 0.82	32.00 ± 2.37	–
	100	0	23.32 ± 2.17	4.20 ± 0.29	42.88 ± 3.99	–
WTIRES	0	0	40.61 ± 3.24	23.68 ± 0.97	24.62 ± 1.96	–
	0	1	NS[a]	NS[a]	NS[a]	–
3DEΔ3F4	0	0	38.17 ± 6.03	80.18 ± 1.88	26.20 ± 4.14	1.4
	0	1	16.92 ± 1.06	30.52 ± 1.53	59.1 ± 3.7	–
3DEΔ3FΔ4	0	0	62.35 ± 8.75	112.40 ± 1.50	16.04 ± 2.25	1.3
	0	1	18.13 ± 1.30	29.25 ± 1.63	55.2 ± 3.9	–
2S	0	0	1.722 ± 0.067	49.03 ± 1.34	580.7 ± 22.6	–
3ABC	0	0	5.866 ± 0.132	85.86 ± 1.14	170.5 ± 3.8	–

[a] Nonspecific binding observed only in these experiments. [b] Hill coefficient.

3DEF4 in that Mg^{2+} ions inhibit viomycin binding (Figure 7a). However, at this $MgCl_2$ concentration, no specific viomycin binding could be observed.

Viomycin binding was also tested in the presence of KCl (see Table 1) and was readily observed to both 3DEF4 and 3EF4 at 50 mM KCl (panels b and d of Figure 6, respectively), but was very weak at 100 mM. In the case of 3DEF4, similar inhibitory effects by K^+ ions may be occurring as was observed with Mg^{2+} ions above. Undoubtedly, K^+ ions present at this high concentration may achieve inhibition of viomycin binding through electrostatic effects. K^+ ions may also have small structural effects on the RNA, different from those of Mg^{2+}, since the former negatively influence viomycin binding to both fragments, unlike the latter.

Viomycin is known to induce intermolecular interactions between certain RNAs (*41*, *42*). Fragments 3DEF4 and 3EF4, at twice the concentration used in binding experiments, were mixed with increasing concentrations of viomycin sulfate on native PAGE (Figure 2c). No viomycin-induced aggregation is observed until viomycin concentrations exceed 250 μM. This concentration is >5-fold higher than the K_d values measured for viomycin binding to both fragments. The results indicate that the observed viomycin binding curves are not due to viomycin-induced aggregation of either 3DEF4 or 3EF4. The presence of 2 mM $MgCl_2$ during electrophoresis did not alter the aggregation pattern (Figure 2d). The inhibition of viomycin binding by magnesium is thus genuine and not an artifact caused by effects on RNA aggregation.

Further evidence that viomycin binding to the IRES has a degree of structural selectivity comes from its comparison to data obtained for the binding of spermine, a far more conformationally mobile molecule bearing four basic amino residues (cf. the three basic residues within viomycin). Not surprisingly, spermine binds to the RNA fragments in microcalorimetry experiments (data not shown) with an apparent dissociation constant in a range similar to that of viomycin. However, there is a very large nonspecific component to the spermine binding data, and it is thus difficult to fit the data and obtain accurate dissociation constants. Inhibition of spermine binding by magnesium is, for the above reasons, also difficult to analyze, but has a significant competitive component, consistent with observations for these molecules in chemical and enzymatic footprinting analyses of the HCV IRES (*18*).

Our studies have thereby located a viomycin binding site in the HCV IRES to the region represented by fragment 3EF4. A component of the binding affinity is electrostatic, and binding is weaker at higher KCl concentrations. The clear effect of Mg^{2+} ions on viomycin binding to 3DEF4 is particularly interesting since, in combination with the thermal melting data, it suggests a scenario whereby Mg^{2+} ions cause a structural transition of the fragment possessing subdomain IIId, hindering access of viomycin to its binding site.

Effect of Mutation or Deletion of Domains IIIf and IV. The two mutants 3DEΔ3F4 and 3DEΔ3FΔ4 (panels d and e of Figure 1, respectively), described earlier, were prepared to test the hypothesis that the viomycin binding site may be located within the pseudoknot region of fragments 3DEF4 and 3EF4. Viomycin binds to 3DEΔ3F4 with a binding constant (26.2 μM) similar to that observed for 3DEF4 and 3EF4 (Figure 7b and Table 1). Deletion of the second half of the pseudoknot along with domain IV, as in 3DEΔ3FΔ4, causes a slight decrease in the dissociation constant for viomycin to 16.0 μM (Figure 7c and Table 1). Again, we observe a better fit to the data when Hill coefficients of 1.3 and 1.4 are fitted for 3DEΔ3F4 and 3DEΔ3FΔ4, respectively. The results suggest that viomycin does not recognize the pseudoknot region of the IRES, but binds elsewhere within subdomains IIIe/f.

The requirement of a Hill coefficient for modeling viomycin binding to 3DEF4, 3DEΔ3F4, and 3DEΔ3FΔ4 is not well understood. It is arguable whether the coefficient figures are significant, although data fits without them result in error margins that are increased up to 25%. It is possible that there is some initial electrostatic interaction between viomycin and the RNA molecules involving subdomain IIId when the molecules are mixed. The apparent cooperativity

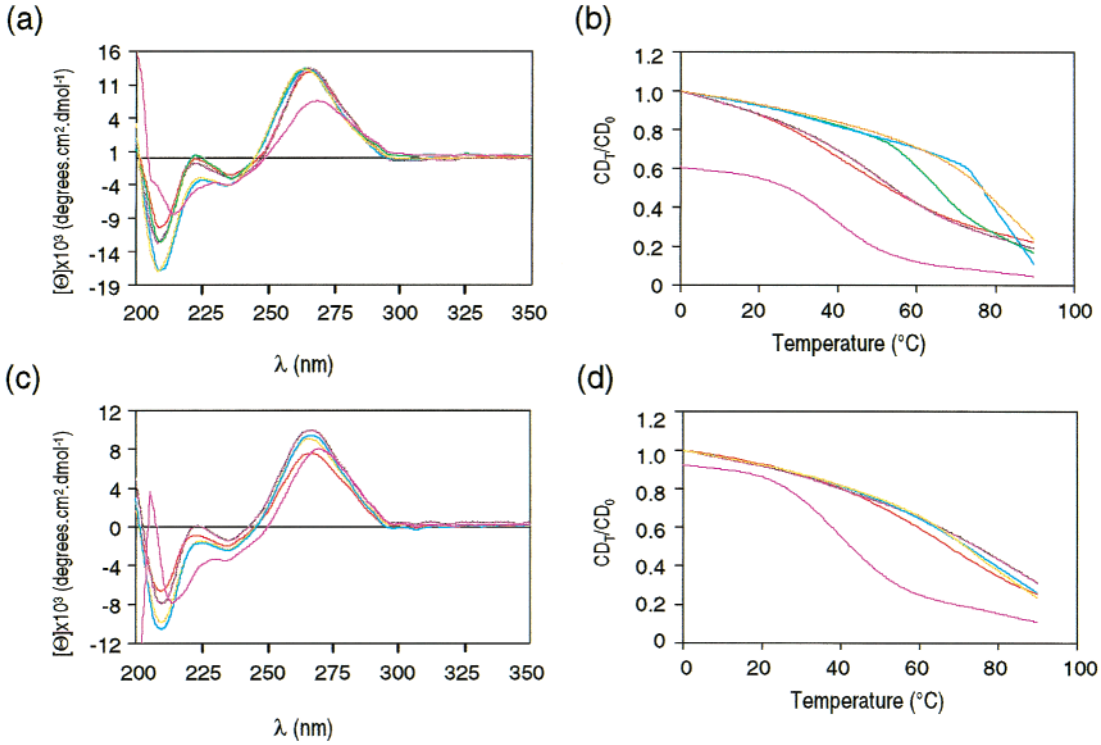

FIGURE 8: Effect of metal ions at 1 mM on the CD spectrum (a) and thermal stability (b) of 3DEF4 and on the CD spectrum (c) and thermal stability (d) of 3EF4. Samples contained ~10 μM RNA in 10 mM HEPES (pH 7.5) and either no metal ions (red) or 1 mM $MgCl_2$ (violet), $MnCl_2$ (green), $CaCl_2$ (light blue), $CoCl_2$ (orange), or $Co(NH_3)_6Cl_3$ (pink).

is not observed for the small fragments that lack subdomain IIId, for WTIRES, or in the presence of $MgCl_2$.

Upon inclusion of 1 mM $MgCl_2$ in the binding experiment, the K_d for viomycin increased slightly for both mutants to 55−60 μM, while the maximum heat of binding, Q_{max}, was decreased (Figure 7 and Table 1). The mutant binding results indicate that viomycin binding is again inhibited by $MgCl_2$. However, compared to that of 3DEF4, the extent of inhibition by $MgCl_2$ at 1 mM has been reduced, since the fitted value for Q_{max} is decreased to 38 and 26% of that in the absence of $MgCl_2$ for 3DEΔ3F4 and 3DEΔ3FΔ4, respectively, rather than to 15% as observed for 3DEF4. The slight increase in the dissociation constant for viomycin observed in the mutants, however, suggests that the inhibition of binding produced by $MgCl_2$ is more complex. It is possible that there are slight structural differences in the mutants which give rise to more complex Mg^{2+} ion-induced inhibition.

Effect of $MgCl_2$ on Pseudoknot Mutant Structures. Addition of $MgCl_2$ to either 3DEΔ3F4 or 3DEΔ3FΔ4 affects the CD spectra (peaks at 265 and 209 nm) of these fragments in a manner similar to that observed for 3DEF4, 3EF4, and WTIRES (Supporting Information), indicating increased base stacking that might represent greater helix stability or formation of tertiary structure. Interestingly, even in the absence of $MgCl_2$, the magnitude of the peak at 223 nm is reduced for 3DEΔ3F4, compared to that of 3DEF4, and almost absent for 3DEΔ3FΔ4. Since the only known difference in these RNA fragments is the destabilization and loss of the pseudoknot interactions, we may speculate that the peak at 223 nm partially represents the extent of tertiary structure interactions within the RNA.

Thermal denaturation of both mutants is also affected by $MgCl_2$. However, the $MgCl_2$ concentration at which sensitivity is observed is reduced in these two mutants, compared to that with fragment 3DEF4, to 0.6−0.7 mM $MgCl_2$. The results suggest that Mg^{2+} ions have a greater stabilizing effect on the structure of mutant RNAs than 3DEF4. Removal of the pseudoknot loop and domain IV may therefore influence the tertiary structure of these RNA fragments, suggesting that these parts are required for normal tertiary folding of the IRES in this region.

The Effect of Other Metal Ions on 3DEF4 and 3EF4 Denaturation Points to a Nonspecific High-Affinity Ion Binding Site of Unusual High Charge Density in 3DEF4. Figure 8a shows the effect of the absence and presence of either $MgCl_2$, $MnCl_2$, $CaCl_2$, or $CoCl_2$ at 1 mM on the CD spectrum of 3DEF4. Both $CaCl_2$ and $CoCl_2$ appear to stabilize base stacking interactions within an A-from helical conformation since both the magnitudes of the 209 and 265 nm peaks are increased in size. Furthermore, the 265 nm peak has also shifted since its maximum is now at 263 nm. $MnCl_2$ appeared to produce an intermediate effect. The metal ions affect 3EF4 RNA structure in the same way (Figure 8c).

The effect of the metal ions on both 3DEF4 and 3EF4 denaturation is shown in panels b and d of Figure 8, respectively. It appears that divalent metal ions other than Mg^{2+} are better able to stabilize 3DEF4 RNA against heat denaturation at equivalent concentrations of the divalent ion. The order of best stabilization ability is Ca > Co > Mn ~ Mg which correlates with their ionic radii (*47*). Of these metal ions, thermal unfolding of 3DEF4 in the presence of 1 mM $MnCl_2$ is not reversible, but this may be due to its interaction with the bases as well as the backbone of the RNA. In the case of 3EF4 RNA, $CoCl_2$ and $CaCl_2$ are able to stabilize the RNA only to thermal denaturation to the same

extent as $MgCl_2$. This difference in behavior of the two fragments in the presence of divalent metal ions again argues for the involvement of subdomain IIId in the structural transition affected by the ions. The correlation of 3DEF4 stability with metal ion radius is indicative of a nonspecific site but one of unusually high negative charge density that can effectively localize metal ions (*48*, *49*).

$Co(NH_3)_6^{3+}$ is a suitable analogue to $Mg(H_2O)_6^{2+}$ since it has a similar ionic radius and covalent geometry (*50*). We find that 1 mM $Co(NH_3)_6^{3+}$ dramatically alters the 3EF4 and 3DEF4 RNA structures and greatly destabilizes them (Figure 8). When the test was carried out at 100 μM, a concentration more appropriate for a trivalent ion, no increase in stabilization of 3DEF4 was observed and denaturation was still not reversible. These observations might indicate that the stabilizing effects of a divalent cation require at least partial direct, rather than solvent shell-mediated, coordination.

DISCUSSION

Mg^{2+} Ions Have No Specific Coordination Site in the RNA Fragments. We conclude from our data that magnesium ions contribute to 3DEF4 RNA stability and do so in two different ways, both of which lead to substantial increases in the apparent T_m of unfolding. Long-range electrostatic forces between the negative charge on RNA and cations are undoubtedly one stabilization effect, conferred by both Mg^{2+} and K^+ ions. However, even in the presence of 100 mM KCl, further Mg^{2+}-dependent stabilization is observed for 3DEF4 but not 3EF4 RNA. 3DEF4 RNA may contain a region of high charge density, such as that created by close juxtaposition of several strands, as in a helix junction or in a segment of triple helix, which is not present in 3EF4 RNA. Indeed, 3DEF4 incorporates an additional subdomain, IIId, which is absent in 3EF4. The sensitivity to the presence of metal ions during denaturation may therefore be due to this subdomain. Previous observations have indicated that the structure of subdomain IIId is not, in isolation, affected by magnesium ions (*21*). A potential ion-dependent long-range interaction of this subdomain with subdomains IIIe and IIIf in the folded IRES structure has been proposed (*18*). If this interaction between IRES subdomains occurs, it would result in a region of higher charge density to which metal ions may bind with unusually high affinity. This type of site has previously been termed an "intermediate" ion binding region (*51*, *52*). In agreement with this definition for metal ion binding holding true for this region of the IRES, the increased stability of fragment 3DEF4 can be conferred by a range of divalent metal ions (*48*), those with the larger ionic radii providing the greatest stability. An exclusive Mg^{2+} binding site where the ion coordinates specifically to a site created by the three-dimensional RNA structure is thus not supported by our observations.

While our thermal denaturation studies did not include the full-length IRES fragment (WTIRES), on native PAGE this RNA migrates as a single band, indicating that it can also fold in the absence of magnesium or other cations. The addition of magnesium ions did not alter the migration of the IRES on a native polyacrylamide gel, even when $MgCl_2$ was also included in the electrophoresis buffer (data not shown). However, it is possible, for an RNA molecule of this size, that different RNA structures may not be detected by PAGE analysis.

The smaller fragments, 3EF4 and 3DEF4, encompassing the pseudoknot region, also usually migrate as a single band in the absence of magnesium. Of these, 3DEF4 is interesting as a minor band is often detectable. The pseudoknot mutant fragments also present additional minor bands. Addition of magnesium ions to renatured RNA appears to promote single-band migration of 3DEF4 and 3DEΔ3FΔ4, while the effects on mutant 3DEΔ3F4 are more complex. Thus, there appears to be a small degree of conformational heterogeneity of RNA fragments possessing subdomain IIId in the absence of magnesium ions. This observation could reflect an equilibrium between at least two conformational states, one of which may be magnesium-stabilized. The more prominent presence of two bands for the mutants might indicate a shift in this equilibrium due to mutation affecting the stability of one conformation.

Mode of Viomycin Binding. In contrast to the nonspecific nature of metal ion binding, the full-length IRES and the subdomain IIIe/f-containing fragments appear to have a specific binding site for viomycin. Viomycin can bind to all these RNA molecules with a similar K_d of 25−55 μM, a binding affinity comparable to that observed for aminoglycosides and derivatives binding to natural targets (*53*, *54*). A large part of the binding affinity is through electrostatic interaction involving the protonated functional groups of viomycin, hence inhibition of binding by increasing concentrations of K^+ ions. Rather than nonspecific electrostatic association of viomycin with the RNA molecules, however, our data and those of others (*43*) point to a more specific shape-selective combination of hydrogen bonding and electrostatics (*55*, *56*), as discussed herein. Of interest in this respect is a recent report that describes a quantitative evaluation of the hydrogen bonding and electrostatic interactions involved in RNA aptamer recognition by neomycin B (*57*). However, such an analysis requires that metal ions do not induce any structural change of the RNA, a condition that large RNAs, including the IRES, are unlikely to fulfill.

Our original basis for testing viomycin binding rested on a strong precedent for this molecule to exhibit selective binding to RNA tertiary structure, specifically, the simplest known tertiary structure, a pseudoknot (*38*, *39*, *43*, *44*). However, the viomycin binding site within the IRES does not appear to include the proposed stem region created by the pseudoknot tertiary interaction, since viomycin retains binding activity toward mutants in which this stem has been altered or removed. Clearly, neither does the binding site include subdomain IIId or domain IV. The remaining region encompassing subdomains IIIe/f is certainly likely to present a complex tertiary structure that viomycin may selectively recognize. A number of possible coaxial stacking arrangements of helices at the IIIef junction are possible, and viomycin may selectively recognize the tertiary structure arrangement in this region. Viomycin binds 3−5 times more weakly to another highly structured IRES fragment, 3ABC (Figure 1), and very weakly to fragment 2S, further supporting location of a relatively high affinity site for viomycin within the IIIe/f region of the full-length IRES. Interestingly, the fragment 3ABC, to which some weak binding of viomycin was observed, also includes a four-way helix junction.

Previous studies on the interaction of small molecules, such as the aminoglycosides, with RNA have suggested that

there are two main modes of binding that enable the small molecules to specifically block RNA function (*29*). In the first, inhibition may occur when a small molecule displaces essential divalent metal ions (*55*, *58*). This type of inhibition is observed when aminoglycoside antibiotics inhibit the activity of several ribozymes in vitro, such as those of the group I introns, the hammerhead and hairpin ribozymes, the human hepatitis delta virus ribozyme, RNase P RNA, and a tRNA (*58*). However, we observe noncompetitive inhibition by Mg^{2+} ions when viomycin binds to 3DEF4 RNA, suggesting that viomycin binds to a site on the RNA which is different from the site where magnesium ions exert their effect (see later discussion).

An alternative type of binding is observed where the aminoglycoside causes a slight distortion in the RNA structure (*29*). This is thought to occur to an internal loop both within the A-site of ribosomal RNA and in the RRE and TAR domains of HIV-1 when neomycin binds to these RNA molecules (*34*, *35*, *59*, *60*). Aminoglycoside-induced structural changes in these RNA molecules may thereby interfere with the binding of the functional substrate. A structural change in RNA is also observed upon binding of neomycin to an aptamer (*62*). Our CD data on IRES−viomycin binding do not indicate a structural change in the RNA, but now that an interaction has been established, closer investigation by NMR or X-ray to address the recognition mechanism more fully is a clear next step.

Mg^{2+}-Induced Structural Rearrangement Blocks Viomycin Binding in the IRES. By examining viomycin binding to the HCV IRES fragments in the presence and absence of magnesium ions, we have indirectly gained further insight into the mode of binding and the tertiary fold of the RNA in the region of subdomains IIIdef. First, binding to 3EF4 is not inhibited by magnesium ions, reinforcing our view that the binding mechanism is structure-selective and not purely electrostatic. This observation also argues against a recognition mechanism that involves simple displacement of divalent metal ions. Indeed, the effect of increasing the magnesium concentration is to enhance, rather than inhibit, viomycin binding to 3EF4. Here the metal ion may be stabilizing the RNA tertiary structure that is selectively bound by viomycin. In the absence of magnesium, viomycin itself has an apparent stabilizing effect on both 3DEF4 and 3EF4. One can argue that binding of the antibiotic stabilizes the RNA conformation that is recognized. However, part of this stabilizing effect is undoubtedly a counterion effect.

Studies of viomycin binding to the larger fragment, 3DEF4, in the presence of magnesium are very revealing from the perspective of the RNA structure and support earlier conclusions regarding the effect of magnesium on the RNA tertiary fold. The noncompetitive inhibition of viomycin binding to fragment 3DEF4 indicates that binding of magnesium ions elsewhere can result in structural changes that interfere with viomycin binding. The contrasting effects of magnesium on viomycin binding to the two fragments implicate subdomain IIId within 3DEF4 in the structural changes that are responsible for the loss of viomycin binding when Mg^{2+} ions are present. Earlier, we suggested that Mg^{2+} ions are stabilizing the RNA fold in this region of the IRES through nonspecific association with an intermediate ion binding region created by a fold that may bring subdomain IIId into the proximity of subdomains IIIe and IIIf and thus create a region of unusually high charge density. It is quite possible that magnesium stabilization of this fold prevents viomycin binding, noncompetitively. Alternatively, Mg^{2+} ions may bind to the high-charge density region of the three-way helical junction at the base of stem IIId and influence the spatial helical arrangement here in a manner that causes hindrance to viomycin binding to region IIIe/f. Metal ions are known to influence RNA folding at helical junctions (*63*, *64*). We would suggest, however, that if Mg^{2+} ions are exerting their inhibitory effect through this alternative means, the noncompetitive inhibition of viomycin binding still demands a steric block that would probably involve subdomain IIId coming close to IIIe/f. Interestingly, previous footprinting data (*18*) indicated strong protection of the region IIIe/f by Mg^{2+}, but no protection in the region of the three-way junction, supporting our first proposal. Also supporting this proposal are the data with mutant RNA fragments.

The structures of the mutant RNA fragments, 3DEΔ3F4 and 3DEΔ3FΔ4, which possess subdomain IIId, are also influenced by magnesium, thus affecting viomycin binding. Significantly, however, the level of inhibition of viomycin binding to these mutants by magnesium is reduced relative to that which occurs with 3DEF4. Thus, a correctly formed pseudoknot stem is required for the normal magnesium-stabilized tertiary fold and might, indeed, participate in an interaction with subdomain IIId. This is the limit to which conclusions can be drawn from data involving the stability of the mutant RNA fragments. We cannot exclude the possibility that removal of the potentially preferred site for tertiary interaction results in quite different RNA structures that present new types and numbers of magnesium binding sites.

Implications for Further RNA Structure Probing and Drug Development. In conclusion, we have established that domains IIIdef and IV of the HCV IRES can fold in the absence of site specific metal ions but that ions play an important role in stabilizing the fold through binding to a region of high charge density brought about by the proximity of helical domains that include subdomain IIId. The tuberactinomycin antibiotic, viomycin, binds to parts of subdomains IIIe and/or IIIf through a combination of electrostatic interaction and structure-selective recognition. Inhibition of viomycin binding to IRES fragments possessing subdomain IIId in a noncompetitive fashion by magnesium has provided evidence of some structure-selective recognition. The mode of inhibition also ties in well with the Mg^{2+} ion stability studies, providing further indirect evidence of an RNA tertiary interaction in this region of the IRES that involves subdomain IIId. Mutations in the pseudoknot stem influence this tertiary interaction. Recent reports identify subdomain IIId, the pseudoknot, and subdomain IV as primary sites of interaction with the 40S ribosomal subunit (*16*, *17*, *19*), clearly more feasible if these regions are close to each other. It would be of interest to model the IRES subdomains IIIe/f and IIId into the globular region of electron density in the cryoelectron microscopy structure (*19*) based on all the data that are now available.

In our studies, viomycin has thus emerged as a useful structural probe. Our data suggest that viomycin is unlikely to bind to the IRES at physiological salt concentrations. However, given the region of the IRES that it targets,

viomycin is by no means excluded as a starting point for synthetic strategies for developing a small, more highly structure-selective molecule that can potentially block HCV translation. Development of such a molecule will require further structural dissection of our observed interaction via analysis of both the elements of RNA structure and functional units of viomycin that are involved. Viomycin and its analogues display extremely well-defined ring conformations (*65*) and are, therefore, ideal platforms for improving our understanding of structure-selective RNA recognition. Analogues of the tuberactinomycins are already available through fermentation technology and semisynthesis (*66*, *67*), and current efforts are directed toward an asymmetric total synthesis of these molecules.

ACKNOWLEDGMENT

We thank Prof. J. McCarthy for his generous donation of the plasmid pCR3.1HCV5′UTR and Prof. T. E. Shrader for his generous donation of the plasmid pT7-911. We also thank Ms. K. Sheehan for preparation of the plasmids and Drs. G. Conn, J. Derrick, and A. Doig for helpful discussions.

SUPPORTING INFORMATION AVAILABLE

Spectra depicting the effect of $MgCl_2$ on the mutants 3DEΔ3F4 and 3DEΔ3FΔ4. This material is available free of charge via the Internet at http://pubs.acs.org.

REFERENCES

1. Clarke, B. (1997) *J. Gen. Virol. 78*, 2397−2410.
2. Smith, D. B., Mellor, J., Jarvis, L. M., et al. (1995) *J. Gen. Virol. 76*, 1749−1761.
3. Ito, T., and Lai, M. M. C. (1997) *J. Virol. 71*, 8698−8706.
4. Rijnbrand, R. C., and Lemon, S. M. (2000) *Curr. Top. Microbiol. Immunol. 242*, 85−116.
5. Hellen, C. U. T., and Pestova, T. V. (1999) *J. Viral Hepatitis 6*, 79−87.
6. Pestova, T. V., et al. (2001) *Proc. Natl. Acad. Sci. U.S.A. 98*, 7029−7036.
7. Krüger, M., Beger, C., Li, Q.-X., Welch, P. J., Tritz, R., Leavitt, M., Barber, J. R., and Wong-Staal, F. (2000) *Proc. Natl. Acad. Sci. U.S.A. 97*, 8566−8571.
8. Honda, M., Ping, L.-H., Rijnbrand, R. C. A., Amphlett, E., Clarke, B., Rowlands, D., and Lemon, S. M. (1996) *Virology 222*, 31−42.
9. Lemon, S. M., and Honda, M. (1997) *Semin. Virol. 8*, 274−288.
10. Wang, C., Le, S. Y., Ali, N., and Siddiqui, A. (1995) *RNA 1*, 526−537.
11. Brown, E. A., Zhang, H., Ping, L.-H., and Lemon, S. M. (1992) *Nucleic Acids Res. 20*, 5041−5045.
12. Honda, M., Brown, E. A., and Lemon, S. M. (1996) *RNA 2*, 955−968.
13. Wang, C., Sarnow, P., and Siddiqui, A. (1994) *J. Virol. 68*, 7301−7307.
14. Deiman, B., and Pleij, C. W. A. (1997) *Semin. Virol. 8*, 166−175.
15. Pestova, T. V., Shatsky, I. N., Fletcher, S. P., Jackson, R. J., and Hellen, C. U. (1998) *Genes Dev. 12*, 67−83.
16. Kolupaeva, V. G., Pestova, T. V., and Hellen, C. U. T. (2000) *J. Virol. 74*, 6262−6250.
17. Kieft, J. S., Zhou, K. H., Jubin, R., and Doudna, J. A. (2001) *RNA 7*, 194−206.
18. Kieft, J. S., Zhou, K., Jubin, R., Murray, M. G., Lau, J. Y. N., and Doudna, J. A. (1999) *J. Mol. Biol. 292*, 513−529.
19. Spahn, C. M. T., Kieft, J. S., Grassucci, R. A., Penczek, P. A., Zhou, K. H., Doudna, J. A., and Frank, J. (2001) *Science 291*, 1959−1962.
20. Beales, L. P., Rowlands, D. J., and Holzenburg, A. (2001) *RNA 7*, 661−670.
21. Klinck, R., Westhof, E., Walker, S., Afshar, M., Collier, A., and Aboul-Ela, F. (2000) *RNA 6*, 1423−1431.
22. Lukavsky, P. J., Otto, G. A., Lancaster, A. M., Sarnow, P., and Puglisi, J. D. (2000) *Nat. Struct. Biol. 7*, 1105−1110.
23. Ecker, D. J., and Griffey, R. H. (1999) *Drug Discovery Today 4*, 420−429.
24. Afshar, M., Prescott, C. D., and Varani, G. (1999) *Curr. Opin. Biotechnol. 10*, 59−63.
25. Sucheck, S. J., and Wong, C. H. (2000) *Curr. Opin. Chem. Biol. 4*, 678−686.
26. Wilson, W. D., and Li, K. (2000) *Curr. Med. Chem. 7*, 73−98.
27. Hermann, T., and Westhof, E. (2000) *Comb. Chem. High Throughput Screening 3*, 219−234.
28. Hermann, T. (2000) *Angew. Chem., Int. Ed. 39*, 1891−1905.
29. Schroeder, R., Waldsich, C., and Wank, H. (2000) *EMBO J. 19*, 1−9.
30. Moazed, D., and Noller, H. F. (1987) *Nature 327*, 389−394.
31. Zapp, M. L., Stern, S., and Green, M. R. (1993) *Cell 74*, 969−978.
32. Mei, H. Y., Galan, A. A., Halim, N. S., Mack, D. P., Moreland, D. W., Sanders, K. B., Truong, H. N., and Czarnik, A. W. (1995) *Bioorg. Med. Chem. Lett. 5*, 2755−2760.
33. Sucheck, S. J., Greenberg, W. A., Tolbert, T. J., and Wong, C. H. (2000) *Angew. Chem., Int. Ed. 39*, 1080−1084.
34. Lacourciere, K. A., Stivers, J. T., and Marino, J. P. (2000) *Biochemistry 39*, 5630−5641.
35. Faber, C., Sticht, H., Schweimer, K., and Rosch, P. (2000) *J. Biol. Chem. 275*, 20660−20666.
36. Marrero, P., Cabanas, M. J., and Modolell, J. (1980) *Biochem. Biophys. Res. Commun. 97*, 1047−1052.
37. Wurmbach, P., and Nierhaus, K. H. (1983) *Eur. J. Biochem. 130*, 9−12.
38. Wank, H., Rogers, J., Davies, J., and Schroeder, R. (1994) *J. Mol. Biol. 236*, 1001−1010.
39. Rogers, J., Chang, A. H., von Ahsen, U., Schroeder, R., and Davies, J. (1996) *J. Mol. Biol. 259*, 916−925.
40. Jenne, A., Hartig, J. S., Piganeau, N., Tauer, A., Samarsky, D. A., Green, M. R., Davies, J., and Famulok, M. (2001) *Nat. Biotechnol. 19*, 56−61.
41. Wank, H., and Schroeder, R. (1996) *J. Mol. Biol. 258*, 53−61.
42. Olive, J. E., De Abreu, D. M., Tastogi, T., Andersen, A. A., Mittermaier, A. K., Beattie, T. L., and Collins, R. A. (1995) *EMBO J. 14*, 3247−3251.
43. Wallis, M. G., Streicher, B., Wank, H., von Ahsen, U., Clodi, E., Wallace, S. T., Famulok, M., and Schroeder, R. (1997) *Chem. Biol. 4*, 357−366.
44. Wank, H., Clodi, E., Wallis, M. G., and Schroeder, R. (1999) *Origins Life Evol. Biosphere 29*, 391−404.
45. Ellinger, T., and Ehricht, R. (1998) *BioTechniques 24*, 718.
46. Johnson, W. C., Jr. (1996) in *Circular Dichroism and the Conformational Analysis of Biomolecules* (Fasman, G. D., Ed.) pp 433−468, Plenum Press, New York.
47. Hay, R. W. (1984) *Bio-inorganic chemistry*, p 24, Halsted Press, Chichester, U.K.
48. Laing, L. G., Gluick, T. C., and Draper, D. E. (1994) *J. Mol. Biol. 237*, 577−587.
49. Misra, V. K., and Draper, D. E. (2000) *J. Mol. Biol. 299*, 813−825.
50. Cowan, J. A. (1993) *J. Inorg. Biochem. 49*, 171−175.
51. Laing, L. G., and Draper, D. E. (1994) *J. Mol. Biol. 237*, 560−576.
52. Gluick, T. C., Wills, N. M., Gesteland, R. F., and Draper, D. E. (1997) *Biochemistry 36*, 16173−16186.
53. Wang, Y., Hamasaki, K., and Rando, R. R. (1997) *Biochemistry 36*, 768−779.
54. Wong, C.-H., Hendrix, M., Manning, D. D., Rosenbohm, C., and Greenberg, W. A. (1998) *J. Am. Chem. Soc. 120*, 8319−8327.
55. Hermann, T., and Westhof, E. (1998) *J. Mol. Biol. 276*, 903−912.

56. Hermann, T., and Westhof, E. (1999) *J. Med. Chem. 42*, 1250−1261.
57. Cowan, J. A., Ohyama, T., Wang, D. Q., and Natarajan, K. (2000) *Nucleic Acids Res. 28*, 2935−2942.
58. Mikkelsen, N. E., Johansson, K., and Kirsebom, L. A. (2001) *Nat. Struct. Biol. 8*, 510−514.
59. Jeneric, O., and Joseph, S. (2000) *J. Mol. Biol. 304*, 707−713.
60. Fourmy, D., Yoshizawa, S., and Puglisi, J. D. (1998) *J. Mol. Biol. 277*, 333−345.
61. Wang, S., Huber, P. W., Cui, M., Czarnik, A. W., and Mei, H.-Y. (1998) *Biochemistry 37*, 5549−5557.
62. Jiang, L., Majumdar, A., Hu, W., Jaishree, T. J., Xu, W., and Patel, D. J. (1999) *Structure 7*, 817−827.
63. Batey, R. T., and Williamson, J. R. (1998) *RNA 4*, 984−997.
64. Walter, F., Murchie, A. I. H., Duckett, D. R., and Lilley, D. M. J. (1998) *RNA 4*, 719−728.
65. Liu, M. L., Toms, H. C., Hawkes, G. E., Nicholson, J. K., and Lindon, J. C. (1999) *J. Biomol. NMR 13*, 25−30.
66. Dirlam, J. P., Belton, A. M., Birsner, N. C., et al. (1997) *Bioorg. Med. Chem. Lett. 7*, 1139−1144.
67. Norcia, L. J. L., Silvia, A. M., Dirlam, J. P., Schnur, R. C., Bergeron, J. M., Retsema, J. A., and Hayashi, S. F. (1999) *J. Antibiot. 52*, 1007−1016.

BI0156310